RADIO CONTINUUM OBSERVATIONS OF THE SNR G65.2 + 5.7 AT 1420 MHz

Y. SOFUE[1] (*), W. REICH[2] and E. M. BERKHUIJSEN[1]

1. Max-Planck- Institut für Radioastronomie, Auf dem Hügel 69, 5300 Bonn 1, Germany

2. Radioastronomisches Institut der Universität Bonn, Auf dem Hügel 71, 5300 Bonn 1, Germany

(*) Speaker: A. von Humboldt Fellow on leave from Department of Physics, Nagoya University, Nagoya, Japan.

Abstract

Radio continuum observations at 1420 MHz of the optical SNR G65.2+5.7 are presented. Intense radio ridges appear to coincide with bright optical filaments. Observed and derived parameters are collected in Table 2. The main characteristics of this SNR are: diameter $\sim$ 75 pc, distance $\sim$ 0.9 kpc, expansion velocity $\gtrsim$ 50 km/s and age $\lesssim$ 2.4 x 10 years. A short comparison with other SNRs is made.

1. Introduction

Recently Gull, Kirshner and Parker (1977) have reported the detection of a filamentary loop structure in optical emission lines centred at $(\alpha,\delta)_{1950} = (19^h31^m, +31°10')$, or $(\ell,b) = (65\overset{\circ}{.}6, +6°)$. It is especially bright in [OIII] and looks like a supernova remnant (SNR) of large angular extent (= 4° x 3°3). One of the brightest filaments has previously been catalogued by Sharpless (1959) as the HII region S91. This filament was noted by van den Bergh (1960) as a candidate SNR filament. Sabbadin and d'Odorico (1976) have shown that also the emission line ratios of Hα, [NII] and [SII] in S91 indicate that this filament is part of a SNR. Sabbadin and d'Odorico as well as Gull et al. found some evidence of radio emission at 820 MHz on the map of Berkhuijsen (1972); Sabbadin and d'Odorico found the radio emission to be more apparent on the 408 MHz map of

Haslam et al. (1974).

In this paper we present new radio continuum data of the area at 1420 MHz with an angular resolution of 11'. The surface brightness - linear diameter (Σ-D) relation and a dynamical model are applied to the SNR.

2. The 1420 MHz Map of G65.2+5.7

The observations were made with the 100-m telescope in Effelsberg of the Max-Planck-Institut für Radioastronomie in April 1977. The resulting map at 1420 MHz is shown in Figure 1 superimposed onto the twenty-minute exposure in [OIII] of Gull et al. (1977). In the radio map, several elongated structures or ridges stand out clearly, i.e. (a) in the north from $\alpha = 19^h32^m$ to 19^h39^m at $\delta \simeq 32°30'$, (b) in the south from $\alpha = 19^h28^m$ to 19^h34^m at $\delta \simeq 29°45'$, and (c) from $\alpha = 19^h34^m$ to 19^h37^m at $\delta \simeq 29°50'$.

The bright radio ridges appear to coincide with the brightest optical filaments. This suggests that the shell of the SNR emits both optical and radio emission from gas of high density at high temperature as well as synchrotron emission from high-energy electrons in a possibly compressed magnetic field. The patchiness of the radio ridges and the point sources in the southern ridge are reminiscent of the Cygnus Loop.

In addition to the bright ridges a small radio ridge coincides with the small but bright filament S94 at $(\alpha,\delta) = (19^h26^m, +31°20')$. On the weaker filaments no radio emission has been detected, putting an upper limit to the brightness temperature $T_b(1420) \lesssim 100$mK. The radio ridge centred at $\alpha = 19^h39^m$, $\delta = 29°30'$ is probably a contamination of galactic plane emission unrelated to the SNR, which influences the map at the lowest latitudes.

3. Spectral Index and Flux Density

(i) Spectral Index between 1420 and 408 MHz

In order to determine the spectral index distribution across the SNR the same area as observed at 1420 MHz was taken from the 408 MHz survey of Haslam et al. (1974). Using a gaussian function the map at 1420 MHz was smoothed to the half-power beamwidth of 37' at 408 MHz.

The average variation of the temperature spectral index β as a function of distance from the centre was studied. The position of the centre and the ellipticity of the loop-like structure were estimated from the lines of maximum intensity of the radio ridges in Figure 1. The centre is at $(\alpha,\delta) = (19^h30^m48 \pm 30^s, +31°5 \pm 2')$, or $(\ell,b) = 65°17 \pm 0.03, +5°73 \pm 0.03)$, and the axial ratio is 1.3 ± 0.1. For both maps at 1420 and 408 MHz the brightness tempe-

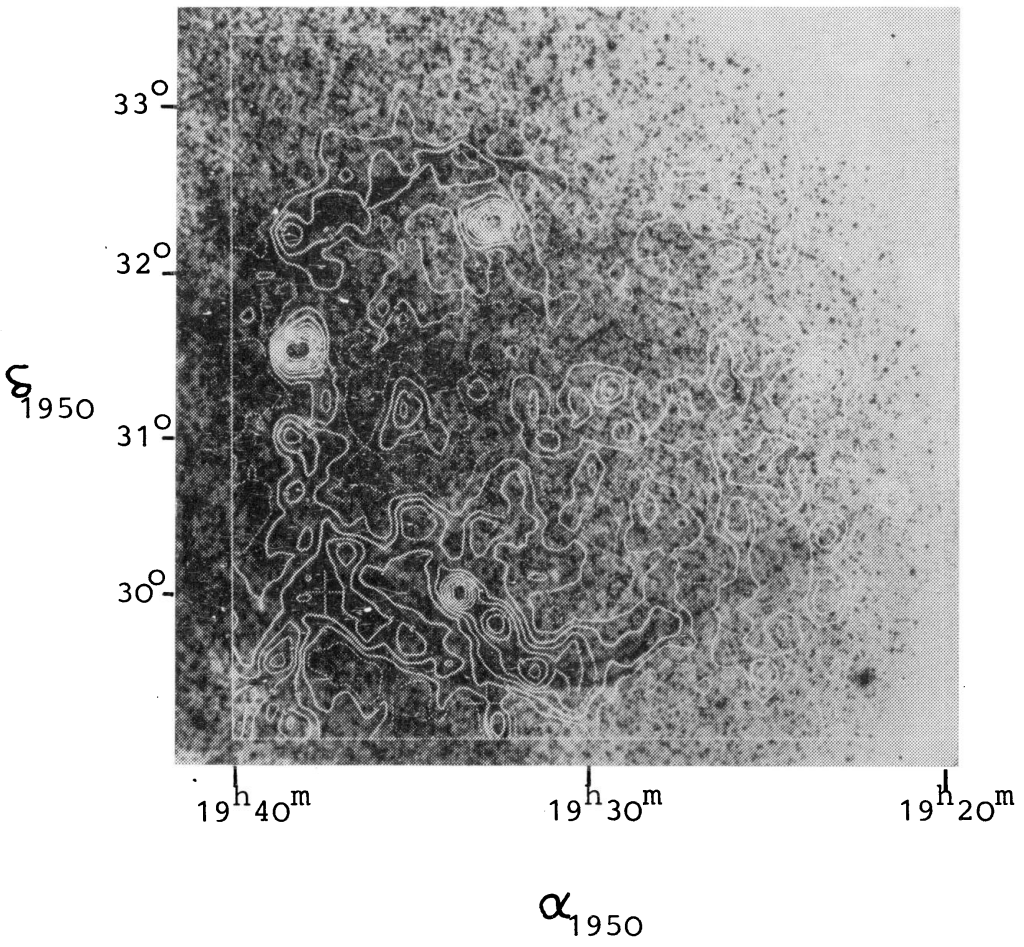

Fig. 1 Contour map of G65.2+5.7 at 1420 MHz with an angular resolution of 11' superimposed onto the twenty-minute exposure in [OIII] of Gull et al. (1977). Contours 0 (dashed) step 1 correspond to levels 0.05 K step 0.15 K in T_b; contour 2 is hatched downhill.

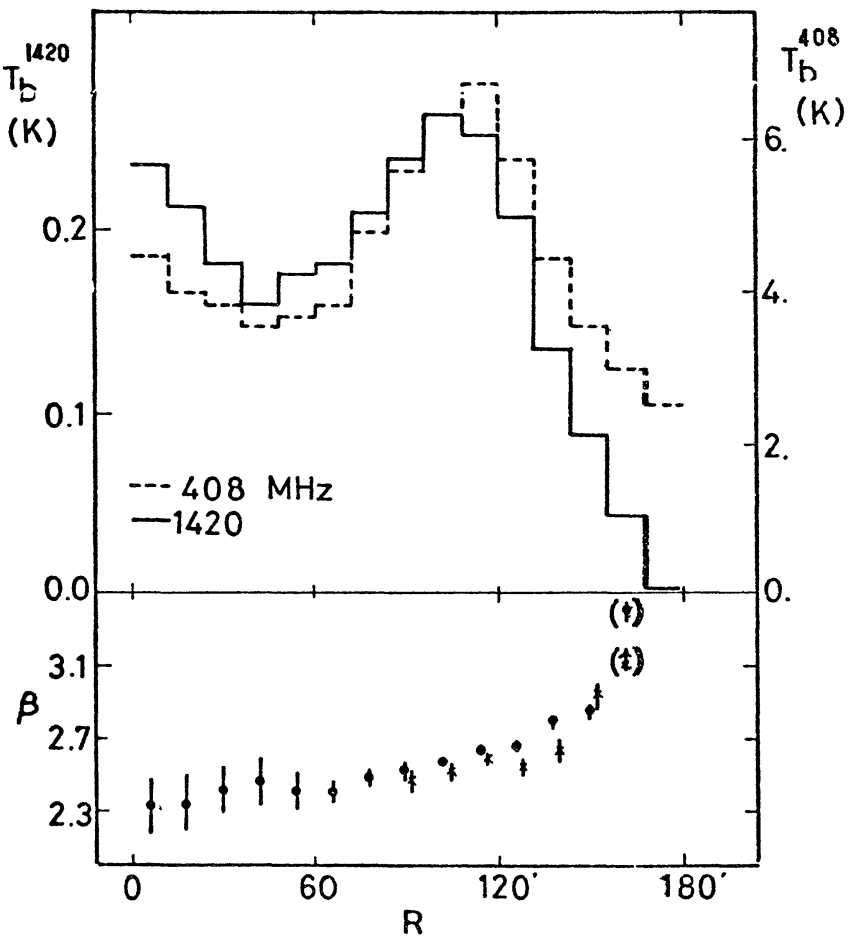

Fig. 2 (a) Distribution of $T_b(1420)$ and $T_b(408)$ after averaging in elliptical rings at distance R from the centre.
(b) Variation of the temperature spectral index β_{1420}^{408} with R derived from the data shown in Figure 2a. Dots - entire area was used; crosses (slightly shifted for clarity) - area $\alpha > 19^h36^m$ not used. Error bars of one standard deviation are shown.

ratures were averaged in elliptical rings around the centre. The resulting cross-cuts and the average β are shown in Figure 2. Apart from some emission near the centre the cross-cuts have the shape typical for SNRs: a relative minimum around the centre, a slow increase to maximum intensity, followed by a steep decrease from the maximum outwards. The emission near the centre is partly due to a source; no optical counterpart is visible. The average spectral index appears to slowly increase from $\beta = 2.34 \pm 0.14$ within 24' from the centre to $\beta = 2.64 \pm 0.02$ at R = 120' and $\beta = 2.96 \pm 0.04$ at R = 150'. However, the increase in β for R > 120' is based on the uncertain outer parts of the maps. The steepening of the spectrum from R = 0' to R = 120' is probably real. (random errors only)

(ii) Integrated flux density

Following Clark and Caswell (1976) the boundary of the elliptically shaped SNR was taken at R = 156' along the "major axis" corresponding to R = 120' along the "minor Axis". The maps at 1420 and 408 MHz were integrated out to this radius yielding the integrated flux densities given in Table 1. The errors quoted are mainly due to uncertainty in the ellipticity; they do not include the uncertainties in the baselevels of the maps. The integrated flux density spectral index is $\alpha_{1420}^{408} = 0.61 \pm 0.05$ (but ± 0.25 if the systematic error is included).

The average surface brightness Σ was derived from the average brightness temperature T_b using the relation $\Sigma = 2 k T_b/\lambda^2$. Interpolation to 1000 MHz gives $\Sigma_{1000} = (1.46 \pm 0.05) \times 10^{-22}$ W m^{-2} ster^{-1} Hz^{-1}. Σ_{408} and Σ_{1000} may be used to find the linear diameter D from the Σ-D relation. Table 2 summarizes the results.

3. Σ-D Relation and Dynamical Model

Applying the four most recent Σ-D relations to the SNR (Ilovaisky and Lequeux, 1972; Berkhuijsen, 1973; Clark and Caswell, 1976; Sabbadin, 1977), taking an average angular diameter of 276' = 4.6, the values for the linear diameter D and distance r are obtained. In view of the large uncertainties we adopt $D = 75^{+50}_{-25}$ pc and $r = 0.9^{+0.6}_{-0.3}$ kpc. These values confirm the estimates of Gull et al. (1977) (D $\sim$ 70 pc). The agreement with the optically determined values of Sabaadin and d'Odorico (1976) (D $\sim$ 34 pc) is also reasonable; it may be noted that the relations they used show a considerable spread, and that they observed line ratios only in one small part of the filaments indicative for the shell. Observations of the line ratios in other parts of the shell are highly desirable.

Gull et al. (1977) have noted that the expansion velocity $V_{exp} \gtrsim 50$ km/s in order to produce the observed strong [OII] lines. From the values of I(H_α)/I(NII) observed in S91 Sabbadin and d'Odo-

rico (1976) estimated $V_{exp} \gtrsim 100$ km/s. However, Lozinskaya (1978) has shown that within old SNRs the expansion velocity of filaments can range from 0 to 150 km/s. Therefore, the value of V_{exp} derived for S91 may not be typical for the SNR as a whole and we adopt $V_{exp} \gtrsim 50$ km/s. With a linear diameter $D = 75^{+50}_{-20}$ pc we then find an age $t \lesssim 2.4^{+1.4}_{-0.8} \times 10$ years and a ratio of total kinetic energy to ambient density $E_o/n_o^{1.12} \gtrsim 1.1^{+2.0}_{-1.0} \times 10^{51}$ ergs $cm^{-3.36}$ (Chevalier, 1974).

Recently Cantó (1977) derived an empirical relation between linear radius, n_o and V_{exp} for the case of a magnetic field $B_o = 3 \times 10^{-6}$ Gauss. Since we observed nonthermal radio emission from the remnant this case may be applicable. Using his Figure 3 we find $n_o \lesssim 9^{+21}_{-7}$ cm^{-3} yielding $E_o \sim 13 \times 10^{51}$ ergs. This energy is ~ 3 times the average E_o of about 20 SNRs obtained by Cantó.

4. Discussion

In Table 3 $^{G}65.2+5.7$ is compared with other SNRs of large size and low radio brightness. The linear diameter and radio surface brightness of G65.2+5.7 are intermediate between those of the Monoceros Loop and S147 and those of the Origem Loop, but the optical appearance, expansion velocity and age are close to those of S147 and the Monoceros Loop. Therefore, G65.2+5.7 seems to be most comparable to these younger remnants, optically in particular to S147; it is larger than S147 probably because of its larger initial energy.

This contribution is a summary of our paper in press for Astronomy and Astrophysics (Reich, Berkhuijsen and Sofue, 1978). See this paper for detailed discussions and further references.

References

Bergh, S. van den, Marscher, A.P., Terzian, Y.: 1973, Astrophys. J. Suppl. 26, 19.
Bergh, S. van den: 1960, Z. f. Astrophysik 51, 15.
Berkhuijsen, E.M.: 1972, Astron. Astrophys. Suppl. 5, 263.

Berkhuijsen, E.M.: 1974, Astron. Astrophys. 35, 429.
Cantó, J.: 1977, Astron. Astrophys. 61, 641.
Chevalier, R.A.: 1974, Astrophys. J. 188, 501.
Clark, D.J., Caswell, J.L.: 1976, Monthly Notices Roy. Astron. Soc. 174, 267.
Gull, T.R., Kirshner, R.P., Parker, R.A.R.: 1977, Astrophys. J. 215, L69.

Haslam, C.G.T., Wilson, W.E., Graham, D.A., Hunt, G.C.: 1974, Astrophys. Suppl 13, 359.
Ilovaisky, S.A., Lequeux, J.: 1972, Astron. Astrophys. 18, 169.
Lozinskaya, T.A.: 1978, Astron. Astrophys. 64, 123.
Reich, W., Berkhuijsen, E.M., Sofue, Y.: 1978, submitted to Astron. Astrophys.
Sabbadin, F.: 1977, Astron. Astrophys. 54, 915.
Sabbadin, F., D'Odorico, S.: 1976, Astron. Astrophys. 49, 119.
Sharpless, S.: 1953, Astrophys. J. 118, 362.

Table 1 Integrated flux and surface brightness

ν (MHz)	S_{int} (Jy)	$\overline{T}_b$ (K)	Σ (10^{-22} W m^{-2} ster^{-1} Hz^{-1})
408	91 ±5	4.93±0.13	2.52 ± 0.07
1420	42.4 ±1.6	0.19±0.01	1.19 ± 0.04

Systematic errors are not included

Table 2 Data on SNR G65.2+5.7

Coordinates of centre		
optical shell	α (1950) (h,m)	19 31
	δ (1950) (°,')	+31 10
	ℓ (°)	65.6
	b (°)	+6
radio shell	α (1950) (h,m,s)	19 30 48±30
	δ (1950) (°,')	31 5±2
	ℓ (°)	65.17±0.03
	b (°)	5.73±0.03
Diameter of optical shell	D (°)	3.3 x 4.0
Diameter between outer half-power points of radio shell	D (°)	4.0 x 5.2
Axial ratio of radio shell		1.3 ± 0.1

Integrated flux density at 1 GHz	S_{int}(Jy)	52 ± 3
Flux density spectral index ($S \propto \nu^{-\alpha}$)	α_{1420}^{408}	0.61 ± 0.25
Average brightness temperature at 1 GHz	$\bar{T}_b$ (K)	0.48 ± 0.03
Average surface brightness at 1 GHz	Σ_{1000}(10^{-22}W m^{-2}ster^{-1}Hz^{-1})	1.46±0.05
Average surface brightness at 408 MHz	Σ_{408}(10^{-22}W m^{-2}ster^{-1}Hz^{-1})	2.52±0.07
Linear diameter of radio shell	D (pc)	75^{+50}_{-25}
Distance to centre of radio shell	r (kpc)	$0.9^{+0.6}_{-0.3}$
Distance above Galactic plane	z (pc)	90^{+60}_{-30}
Expansion velocity	V_{exp}(km/s)	$\gtrsim 50$
Age	t (10^5 years)	$\lesssim 2.4^{+1.4}_{-0.8}$
Assumed ambient magnetic field	B_o (10^{-6} Gauss)	3
Ambient density	n_o (cm^{-3})	9^{+21}_{-7}
Initial energy	E_o (10^{51} ergs)	~ 13

Table 3 Comparison of G65.2+5.7 with similar SNRs

Variable	Monoceros Loop	S147	G65.2+5.7	Origem Loop	References
Optical appearance	faint HII ring weak filaments	shell of long filaments	shell of long filaments, strong |OIII/Hα|	some bright HII regions, no filaments	1,1,4,6
ℓ, (°)	205.5, +0.2	180.0, -1.7	65.2, +5.7	194.7, +0.4	2,2,7,6
Σ_{408} (10^{-22}Wm^{-2}ster^{-1}Hz^{-1})	4.1 ± 0.4	5.2 ± 0.5	2.5 ± 0.1	1.1 ± 0.5	2,2,7,6
D (pc)	49 ±10	51 ± 10	75^{+50}_{-25}	116 ± 52	2,2,7,6
r (kpc)	0.7 ± 0.2	1.0 ± 0.2	$0.9^{+0.6}_{-0.3}$	1.1 ± 0.5	2,2,7,6
V_{exp} (km/s)	50 ± 10	50 ± 10	$\gtrsim$50	∼20	3,3,4,6
t (10^5 years)	1.5 ± 0.4	1.5 ± 0.5	$\lesssim 2.4^{+1.4}_{-0.8}$	∼10	8,8,8,8
$E_o/n_o^{1\ 12}$ (10^{51}erg cm$^{-3,36}$)	0.3 ± 0.2	0.3 ± 0.2	$\gtrsim 1.1^{+2.0}_{-1.0}$	∼1	8,8,8,8
n_o (cm^{-3})	14^{+22}_{-12}	12^{+19}_{-10}	9^{+21}_{-7}	∼0.5 [6]	9,9,7,6 [9]
E_o (10^{51} erg)	5 ± 1	5 ± 1	13 ± 2	∼0.5 [6]	

(1) van den Bergh et al. (1973); (2) Clark, Caswell (1976); (3) Lozinskaya (1978); (4) Gull et al. (1977); (5) Sabbadin, D''Odorico (1976); (6) Berkhuijsen (1974); (7) this paper ; (8) derived from 0.3 R $=V_{exp}$ t 10^6 pc and E_o $10^{50} = 5.3\ 10^{-7}\ n_o^{1.12}\ V_{exp}^{1.4}\ R^{3.12}$ ergs, both holding after the shell has been formed (Chevalier, 1974); (9) Cantó (1977), Figure 3; a magnetic field of 3 x 10^{-6} Gauss has been assumed.